

## DYNAMICAL CONSTRAINTS ON THE ORIGIN OF HOT AND WARM JUPITERS WITH CLOSE FRIENDS

FABIO ANTONINI<sup>1</sup>, ADRIAN S. HAMERS<sup>2</sup> AND YORAM LITHWICK<sup>1</sup>

(1) Center for Interdisciplinary Exploration and Research in Astrophysics (CIERA) and Department of Physics and Astrophysics, Northwestern University, Evanston, IL 60208; (2) Leiden Observatory, Niels Bohrweg 2, Leiden, 2333CA, The Netherlands

*Draft version March 11, 2021*

### ABSTRACT

Gas giants orbiting their host star within the ice line are thought to have migrated to their current locations from farther out. Here we consider the origin and dynamical evolution of observed Jupiters, focusing on hot and warm Jupiters with outer friends. We show that the majority of the observed Jupiter pairs (twenty out of twenty-four) will be dynamically unstable if the inner planet was placed at  $\gtrsim 1$  AU distance from the stellar host. This finding is at odds with formation theories that invoke the migration of such planets from semi-major axes  $\gtrsim 1$  AU due to secular dynamical processes (e.g., secular chaos, Lidov-Kozai oscillations) coupled with tidal dissipation. In fact, the results of  $N$ -body integrations show that the evolution of dynamically unstable systems does not lead to tidal migration but rather to planet ejections and collisions with the host star. This and other arguments lead us to suggest that most of the observed planets with a companion could not have been transported from further out through secular migration processes. More generally, by using a combination of numerical and analytic techniques we show that the high- $e$  Lidov-Kozai migration scenario can only account for less than 10% of all gas giants observed between 0.1 – 1 AU. Simulations of multi-planet systems support this result. Our study indicates that rather than starting on highly eccentric orbits with orbital periods above one year, these “warm” Jupiters are more likely to have reached the region where they are observed today without having experienced significant tidal dissipation.

### 1. INTRODUCTION

The observed abundance of Jupiter-size planets orbiting interior to the ice-line around their stars poses a challenge to our current understanding of planet formation (Wright et al. 2012). Close-in planets ( $\lesssim 1$  AU) are typically thought to have formed beyond the ice-line where large, icy cores can grow and accrete, and to have moved within 1 AU later on. Possible mechanisms for migration invoke gentle disk migration (e.g., Goldreich & Tremaine 1980; Lin et al. 1996) or tidal interaction with the stellar host that gradually removes energy from the planet orbit. In this latter model the interaction with an external perturber (e.g., a star, a planet companion) moves the planet onto a highly eccentric orbit so that efficient tidal circularization can take place (e.g., Rasio & Ford 1996; Wu & Murray 2003; Wu & Lithwick 2011; Naoz et al. 2011).

Migration scenarios must account for the existence of both hot Jupiters (HJs; gas giants orbiting within 0.1 AU of their host stars) and warm Jupiters (WJs; orbiting in the region from 0.1 to 1 AU). WJs are giant planets observed within the so called period “valley”, corresponding to the dip in the giant planet orbital period distribution from roughly  $P = 10$  to 100 days (Santerne et al. 2015). Thus, WJs are interior to both the ice-line and the observed pileup of giant planets beyond 1 AU. While most HJs have nearly zero eccentricities, WJs have a range of eccentricities with a few being on highly eccentric ( $\gtrsim 0.8$ ) orbits (e.g., Dawson & Murray-Clay 2013).

Although HJs and WJs appear to be separated in their period and eccentricity distributions it has been suggested that they might share a common origin. A possibility is that both HJs and WJs migrated inward through high- $e$  migration processes such as secular chaos and Lidov-Kozai (LK) cycles coupled with tidal fric-

tion (e.g., Dong et al. 2014; Dawson & Chiang 2014; Frewen & Hansen 2016). In this scenario the HJ orbits have been fully circularized by tidal friction, while WJs are still on their way to become HJs and are experiencing large amplitude eccentricity oscillations induced by an external perturber. In fact, most gas giants observed in the period valley have observed eccentricities that are too small for significant tidal evolution, but this can be understood if they are currently near the low- $e$  phase of a LK cycle, while periodically attaining high eccentricities and thereby experiencing significant tidal dissipation.

In this paper we examine whether high- $e$  migration models are consistent with the observed properties of the WJ population. We based our analysis on (mostly) radial-velocity data from the exoplanet database at <http://exoplanets.org> (Wright et al. 2011). In particular, we focus on planets that have a detected outer companion and that orbit their stellar host interior to 1 AU. We use both a high precision three-body integrator as well as an orbit average secular code to produce synthetic populations of migrating planets. By comparing our results to observations we are able to address whether the giant planets observed in the period valley could have formed through secular migration processes.

We find that secular processes do cause giant planets to migrate within the radial range 0.1 – 1 AU, however the orbital properties of the migrating planets are not consistent with what is observed. Our results are consistent with less than 10% of all gas giants observed in the period valley having migrated through tidal dissipation. We note that our results are somewhat complementary to those of Huang et al. (2016). These authors recently used Kepler transit data to show that HJs and WJs are distinct in their respective fractions of sub-Jovian companions. They found that HJs as a whole do not have any

detectable inner or outer planetary companions with periods inward of 50 days. In stark contrast, half of the WJs in their sample have small companions. Motivated by this discovery and by additional arguments, Huang et al. (2016) proposed that a large fraction of WJs are formed in-situ.

The paper is organized as follows. In Section 2 we consider all planets within 1AU that have a detected outer companion and address the dynamical stability of these systems. In Section 3 we describe our numerical methods. In Section 4 we describe the results of the  $N$ -body integrations that we used to study the dynamical evolution of systems close to the stability boundary. In Sections 5 and 6 we study the dynamical evolution of planets undergoing secular migration and their resulting orbital distribution. Section 7 summarizes our main results.

## 2. STABILITY

In this Section we discuss the stability of observed Jupiter pairs hosting HJs and WJs. In particular, we examine whether the HJ or WJ could have reached its current orbit via high- $e$  migration, or whether its having a high- $e$  and  $a \sim 1\text{AU}$  in the past would instead have made the system dynamically unstable.

The majority of WJs are far enough from their stellar hosts that they are not expected to experience significant tidal dissipation. However, if the eccentricity of the WJs are experiencing large amplitude LK oscillations induced by an external perturber, then they might be currently at the low- $e$  phase of a LK cycle. Over a secular timescale they might access a periapsis separation such that  $a_1(1 - e_1^2) < a_{\text{cr}} \approx 0.1\text{AU}$ , within which tidal dissipation will cause efficient migration. In this scenario the WJs have to be accompanied by a strong enough perturber to overcome Schwarzschild precession. Note that at  $\sim 0.1\text{AU}$ , the additional precession due to tides are negligible compared to Schwarzschild precession for typical hosts.

Dong et al. (2014) consider the secular migration scenario for WJs. At the quadrupole level of approximation they derive an analytic upper limit on the outer perturber separation by requiring the WJ to reach  $a_1(1 - e_1^2) < a_{\text{cr}}$  during LK oscillations:

$$\frac{a_2\sqrt{1 - e_2^2}}{a_1} \lesssim \left(\frac{8GM_\star}{c^2 a_1}\right)^{-1/3} \left(\frac{M_\star}{M_2}\right)^{-1/3} \quad (1)$$

$$\left[2e_1^2 + 3\left(1 - \frac{a_{\text{cr}}}{a_1}\right)\right]^{1/3} \left(\sqrt{\frac{a_1}{a_{\text{cr}}}} - \frac{1}{\sqrt{1 - e_1^2}}\right)^{-1/3}$$

where  $M_\star$  is the mass of the host star,  $M_2$  the mass of the outer perturber and  $a_1$  ( $a_2$ ) and  $e_1$  ( $e_2$ ) are the semi-major axis and eccentricity of the inner (outer) planet. In the limit  $a_1 \gg a_{\text{cr}}$  and  $e_1 \rightarrow 0$ , Equation (1) becomes

$$\frac{a_2\sqrt{1 - e_2^2}}{a_1} \lesssim \left(\frac{8GM_\star}{c^2\sqrt{a_1 a_{\text{cr}}}}\right)^{-1/3} \left(\frac{M_\star}{M_2}\right)^{-1/3} \approx 20 \left(\frac{M_2}{M_{\text{Jupiter}}}\right)^{1/3}$$

$$\times \left(\frac{M_\star}{M_\odot}\right)^{-2/3} \left(\frac{a_1}{0.2\text{AU}}\right)^{1/6} \left(\frac{a_{\text{cr}}}{0.1\text{AU}}\right)^{1/6}.$$

Using the above equations Dong et al. (2014) concluded that “for a WJ at 0.2AU, a Jupiter perturber is required at  $\lesssim 3\text{AU}$ ”.

Previous work did not consider the stability of the initial configurations that can lead to the formation of a WJ in the secular migration scenario. In addition to the condition Equation (1) one must require the planetary system to be dynamically stable in its initial configuration, i.e., before tidal dissipation has significantly shrank the orbit of the inner planet.

We compare the observed systems configurations to various stability criteria. We consider the criterion (Petrovich 2015)

$$\frac{a_2(1 - e_2)}{a_1(1 + e_1)} > 2.4 \left[\max\left(\frac{M_2}{M_\star}, \frac{M_1}{M_\star}\right)\right]^{1/3} \left(\frac{a_2}{a_1}\right)^{1/2} + 1.15, \quad (3)$$

which is applicable to planet-star mass ratios  $10^{-4} - 10^{-2}$  and mutual inclinations up to  $40^\circ$ . This criterion is essentially equivalent to that of Eggleton & Kiseleva (1995):

$$\frac{a_2(1 - e_2)}{a_1(1 + e_1)} > 1 + 3.7 \left(\frac{M_2}{M_\star}\right)^{1/3} + \frac{2.2}{1 + (M_2/M_\star)^{-1/3}} + 1.4 \left(\frac{M_1}{M_\star}\right)^{1/3} \frac{(M_2/M_\star)^{-1/3} - 1}{1 + (M_2/M_\star)^{-1/3}}. \quad (4)$$

Systems that do not satisfy the condition Equation (3) and (4) are expected to be unstable leading to either ejections or collisions. It can be shown by combining Equation (2) and Equation (3) and taking the limit  $e_1 \rightarrow 1$  in this latter equation that for a Jupiter mass perturber there are no stable configurations which allow the formation of a WJ at  $\lesssim 0.3\text{AU}$ .

Another often adopted stability criterion is that of Mardling & Aarseth (2001),

$$\frac{a_2(1 - e_2)}{a_1} > 2.8 \left[\left(1 + \frac{M_2}{M_\star}\right) \frac{1 + e_2}{(1 - e_2)^{1/2}}\right]^{2/5}. \quad (5)$$

Note that the Mardling & Aarseth (2001) criterion does not include a dependence on the inner planet orbital eccentricity, and was derived for cases in which the mass ratio between the inner and outer binary is not much different from unity. For these reasons, we consider Equations (3) and (4) more accurate for the two planet systems we are considering. The results of our simulations confirm this.

In Figure 1 we compute the stability boundaries defined above by adopting the observed orbital parameters of HJs and WJs with a detected companion. The full sample of planets we considered is presented in Table 1. We selected systems with two giant planets and that host a Jupiter planet with mass  $M_1 \sin i \geq 0.5M_{\text{Jupiter}}$  and semi-major axis  $< 1\text{AU}$ . The left panel shows the inner Jupiter semi-major axis as a function of the critical inner-planet semi-major axis which would render the system unstable according to Equations (3) and (5). At larger semi-major axis the system will be unstable and any secular process leading to high- $e$  migration is likely to be suppressed. Since a secular migration scenario requires the inner Jupiter to have initially an extremely large eccentricity we take the limit  $e_1 \rightarrow 1$  when evaluating Equation (3). Also, we added a factor 0.5 to right hand side of Equation (3), which according to Petrovich (2015) corresponds approximately to 95% chance for a

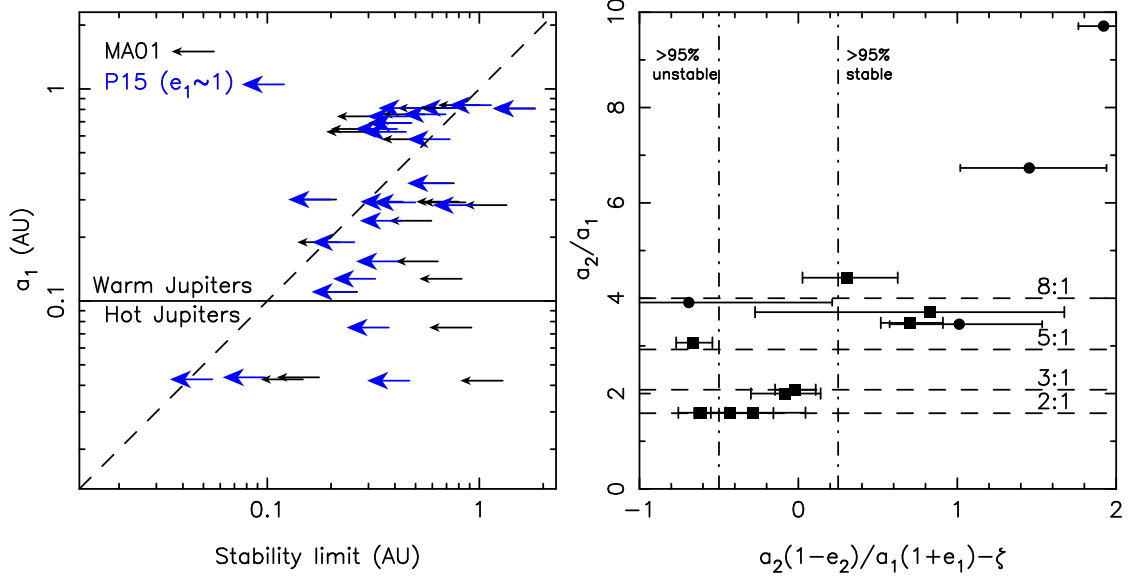


FIG. 1.— The left panel gives the semi-major axis of HJs and WJs with observed companions plotted as a function of the inner planet semi-major axis above which the system will be unstable. The inner planet must have been to the left of the tip of each arrow during its high  $e$  migration (assuming it formed via high  $e$  migration); otherwise, it would have been dynamically unstable according to Equation (5) (black arrows) and Equation (3) (blue arrows). The stability limit imposed by Equation (3) was computed taking the limit  $e_1 \rightarrow 1$  and adding a factor 0.5 to the right hand side which approximately corresponds to 95% chance for a system to be unstable over  $10^8$  years of evolution. Systems that are to the left of the dashed line are dynamically unstable according to the stability criteria we considered. The right panel shows the stability boundary in Equation (3) as a function of the semi-major axis ratio  $a_2/a_1$  for our sample of two-planet systems; here  $\zeta = 2.4[\max(\mu_2, \mu_1)]^{1/3} \sqrt{a_2/a_1} + 1.15$ . The vertical dot-dashed line indicates the region for which > 95% of the systems to be unstable (stable). The horizontal dashed lines indicate the position of some of the strongest mean-motion resonances. Square (circle) symbols are systems with semi-major axis  $a_1 \geq 0.5$  AU ( $\leq 0.5$  AU).

system to be unstable over  $10^8$  years of evolution.

From the left panel of Figure 1 we see that most Jupiters at  $0.6 \leq a_1 \leq 0.8$  AU are close or above the stability boundary defined by the dashed line. Clearly this simple fact is difficult to reconcile with a high- $e$  migration model for these planets, suggesting that such systems are unlikely to have experienced significant tidal migration from further out. Note that in Figure 1 the stability boundaries were computed using the minimum mass for the planets. If the planet orbits were significantly tilted with respect to the line of sight, the planet masses could be significantly larger which will further push the stability boundary towards smaller semi-major axes.

In the region  $0.1 \leq a_1 \leq 0.6$  AU the two adopted stability criteria start to give somewhat different values for the limiting initial  $a_1$  implied by our stability argument. According to Equation (3), 9 out of 10 WJs within 0.6 AU could not have migrated from  $a_1 \gtrsim 1$  AU as they would have been dynamically unstable otherwise. According to Equation (5) instead, 8 out of 10 WJs within 0.6 AU would be dynamically unstable at  $a_1 \gtrsim 1$  AU suggesting that they could not have migrated from these distances. Two (HAT-P-13 and Kepler-424) of the four HJs with known companion have very strong constraints on their maximum separation required by stability, implying that if they formed through secular migration they must have been initially at  $\lesssim 0.2$  AU.

A possibility is that WJs formed by interactions with a planetary companion and began tidal circularization interior to 1 AU after multiple scatterings. However, among the ten WJs detected within  $\lesssim 0.5$  AU only two are above the stability boundary given by Equation (3) when setting  $a_1 = 0.6$  AU and taking the limit  $e_1 \rightarrow 1$ ; these planets are HD-37605c and HD-163607b. There are

also a few systems that at  $a_1 = 0.6$  AU would be classified as unstable according to Equation (3) but are just above the stability boundary defined by Equation (5). These systems are HD-38529, HD-74156, HD-13908 and HD-168443. Further dynamical constraints on a possible high- $e$  migration scenario for some of these systems are presented in the next sections.

In the right panel of Figure 1 we show the stability boundary in Equation (3) for our sample of two-planet systems. We also identify the region where 95% of the systems according to Equation (3) would be unstable after  $10^8$  yr of evolution. Surprisingly, some of these planets appear to be well inside the dynamically unstable region. As also noted by Petrovich (2015), however, the stability of these systems might be promoted by mean-motion resonances (some of which are indicated in Figure 1). In any case, it is hard to imagine how these planets could have been transported from further out through secular migration processes.

The stability analysis shown in Figure 1 suggests that most WJs and HJs with observed companions cannot have migrated to their current location via tidal dissipation from  $a_1 \approx 1$  AU. This idea is further explored and supported by the analysis presented in the following sections.

In Table 1 we give the orbital parameters of observed two planet systems with an inner WJ or HJ and summarize the results of our stability analysis. Importantly, and contrary to previous work (Dawson & Chiang 2014), we note that our analysis disfavors a high migration origin for most WJs with a companion, including those having a finite orbital eccentricity ( $e_1 \gtrsim 0.2$ ).

### 3. NUMERICAL METHODS AND TEST CASES

TABLE 1  
OBSERVED ORBITAL ELEMENTS OF DETECTED SYSTEMS COMPRISING WARM ( $0.1 \leq a \leq 1\text{AU}$ ) AND HOT ( $a < 0.1\text{AU}$ ) JUPITERS AND THEIR CLOSE FRIEND. ONLY SYSTEMS WITH TWO GIANT PLANETS WERE CONSIDERED.

System	$a_1$ (AU)	$e_1$	$M_1 \sin i_1$ ( $M_{\text{Jupiter}}$ )	$a_2$ (AU)	$e_2$	$M_2 \sin i_2$ ( $M_{\text{Jupiter}}$ )	$r_{\text{cr}}$ (AU)	High- $e$ migration
HD82943	$0.742 \pm 0.0129$	$0.425 \pm 0.03$	$1.59 \pm 0.103$	$1.185 \pm 0.022$	$0.203 \pm 0.065$	$1.589 \pm 0.097$	0.50	$\times \times$
HD12661	$0.838 \pm 0.0177$	$0.3768 \pm 0.0077$	$2.34 \pm 0.101$	$2.919 \pm 0.064$	$0.031 \pm 0.022$	$1.949 \pm 0.092$	1.19	$\checkmark$
HD169830	$0.813 \pm 0.0136$	$0.310 \pm 0.01$	$2.89 \pm 0.102$	$3.60 \pm 0.35$	$0.330 \pm 0.02$	$4.06 \pm 0.35$	0.87	$\times$
HD207832	$0.570 \pm 0.02$	$0.13 \pm 0.05$	$0.564 \pm 0.065$	$2.11 \pm 0.1$	$0.27 \pm 0.1$	$0.73 \pm 0.161$	0.73	$\times$
HD73526	$0.647 \pm 0.011$	$0.190 \pm 0.05$	$2.86 \pm 0.172$	$1.028 \pm 0.0177$	$0.140 \pm 0.09$	$2.42 \pm 0.167$	0.43	$\times \times$
HD155358	$0.627 \pm 0.0168$	$0.170 \pm 0.03$	$0.819 \pm 0.068$	$1.001 \pm 0.027$	$0.16 \pm 0.1$	$0.807 \pm 0.056$	0.47	$\times \times$
HD202206	$0.812 \pm 0.0164$	$0.4350 \pm 0.001$	$16.82 \pm 0.68$	$2.490 \pm 0.055$	$0.267 \pm 0.021$	$2.33 \pm 0.127$	0.65	$\times \times$
HD60532	$0.759 \pm 0.0176$	$0.280 \pm 0.03$	$1.035 \pm 0.069$	$1.580 \pm 0.04$	$0.020 \pm 0.02$	$2.46 \pm 0.146$	0.73	$\times \times$
HD134987	$0.808 \pm 0.016$	$0.2330 \pm 0.002$	$1.563 \pm 0.062$	$5.83 \pm 0.33$	$0.120 \pm 0.02$	$0.805 \pm 0.046$	1.93	$\checkmark$
HD37605	$0.283 \pm 0.047$	$0.6767 \pm 0.0019$	$2.80 \pm 0.93$	$3.82 \pm 0.64$	$0.013 \pm 0.013$	$3.4 \pm 1.12$	1.34	$\checkmark$
HD163607	$0.3592 \pm 0.006$	$0.730 \pm 0.02$	$0.769 \pm 0.041$	$2.418 \pm 0.041$	$0.120 \pm 0.06$	$2.29 \pm 0.108$	0.76	$\times$
HD147018	$0.2389 \pm 0.004$	$0.486 \pm 0.0081$	$2.127 \pm 0.076$	$1.923 \pm 0.039$	$0.133 \pm 0.011$	$6.59 \pm 0.29$	0.62	$\times$
HD74156	$0.2915 \pm 0.0049$	$0.630 \pm 0.01$	$1.773 \pm 0.09$	$3.900 \pm 0.067$	$0.380 \pm 0.02$	$8.25 \pm 0.36$	0.86	$\times$
HD13908	$0.1538 \pm 0.0026$	$0.046 \pm 0.022$	$0.865 \pm 0.035$	$2.034 \pm 0.042$	$0.120 \pm 0.02$	$5.13 \pm 0.25$	0.64	$\times /$
HD168443	$0.2939 \pm 0.0049$	$0.529 \pm 0.024$	$7.70 \pm 0.29$	$2.853 \pm 0.048$	$0.2113 \pm 0.0017$	$17.39 \pm 0.58$	0.80	$\times$
HD159243	$0.1104 \pm 0.0018$	$0.020 \pm 0.018$	$1.130 \pm 0.05$	$0.805 \pm 0.0171$	$0.075 \pm 0.05$	$1.90 \pm 0.13$	0.27	$\times /$
HD38529	$0.1272 \pm 0.0021$	$0.244 \pm 0.028$	$0.803 \pm 0.033$	$3.600 \pm 0.06$	$0.3551 \pm 0.0074$	$12.26 \pm 0.42$	0.83	$\times /$
HD9446	$0.1892 \pm 0.0063$	$0.200 \pm 0.027$	$0.699 \pm 0.065$	$0.654 \pm 0.022$	$0.060 \pm 0.06$	$1.82 \pm 0.172$	0.27	$\times /$
TYC-1422								
-614-1	$0.689 \pm 0.036$	$0.06 \pm 0.02$	$2.5 \pm 0.4$	$1.396 \pm 0.073$	$0.048 \pm 0.014$	$10 \pm 1$	0.51	$\times \times$
K-432	$0.301 \pm 0.065$	$0.5134 \pm 0.0089$	$5.5 \pm 2.4$	$1.18 \pm 0.25$	$0.498 \pm 0.059$	$2.4 \pm 1.04$	0.21	$\times \times$
K-424	$0.04365 \pm 0.00078$	$0.002 \pm 0.071$	$1.034 \pm 0.099$	$0.724 \pm 0.0137$	$0.319 \pm 0.081$	$7.04 \pm 0.58$	0.18	$\times$
HAT-P-13	$0.04269 \pm 0.00087$	$0.0133 \pm 0.0041$	$0.851 \pm 0.035$	$1.226 \pm 0.025$	$0.6616 \pm 0.0054$	$14.27 \pm 0.69$	0.14	$\times$
HD217107	$0.0750 \pm 0.00125$	$0.1267 \pm 0.0052$	$1.401 \pm 0.048$	$5.33 \pm 0.2$	$0.517 \pm 0.033$	$2.62 \pm 0.15$	0.91	$\checkmark$
HD187123	$0.04209 \pm 0.0007$	$0.0103 \pm 0.0059$	$0.510 \pm 0.0173$	$4.83 \pm 0.37$	$0.252 \pm 0.033$	$1.94 \pm 0.152$	1.30	$\checkmark$

Orbital parameters of known WJs and HJs with a detected Jupiter companion. We selected systems with two giant planets, hosting a Jupiter planet with mass  $M_1 \sin i \geq 0.5M_{\text{Jupiter}}$  and semi-major axis  $< 1\text{AU}$ . The value of  $r_{\text{cr}}$  is the maximum value of the inner planet semi-major axis above which the two planet system will be dynamically unstable, which we computed as the maximum value between the two stability boundaries obtained via Equation (3) and Equation (5). The stability limit imposed by Equation (3) was computed taking the limit  $e_1 \rightarrow 1$  and adding a factor 0.5 to the right hand side which corresponds to 95% chance for a system to be unstable over  $10^8$  years. Systems with  $r_{\text{cr}} \lesssim 1\text{AU}$  ( $r_{\text{cr}} \lesssim a_1$ ) are indicated with a  $\times$  ( $\times \times$ ) symbol in the last column. Our stability analysis disfavors a high-migration scenario for the formation of these systems. Systems with a low eccentricity,  $e_1 \leq 0.3$ , at  $0.1 \leq a_1 \leq 0.3\text{AU}$  are indicated with a  $/$  symbol. Our analysis of Section 5.1 disfavors a high-migration scenario for these systems as well. Systems for which our study does not rule out a secular migration origin are indicated with a  $\checkmark$  symbol. The observations reported at <http://exoplanets.org> (Wright et al. 2011) include data from Mayor et al. (2004); Correia et al. (2005); Tinney et al. (2006); Desert et al. (2008); Wright et al. (2009); Ségransan et al. (2010); Hébrard et al. (2010); Winn et al. (2010); Jones et al. (2010); Pilyavsky et al. (2011); Meschiari et al. (2011); Wang et al. (2012); Haghighipour et al. (2012); Giguere et al. (2012); Robertson et al. (2012); Tan et al. (2013); Endl et al. (2014); Moutou et al. (2014); Niedzielski et al. (2015); Quinn et al. (2015).

In what follows we study the evolution of Jupiter like planets around a solar like star induced by the gravitational interaction with an outer Jupiter companion. Our goal is to put constraints on the origin of some of the observed Jupiters within 1AU focusing mostly on planets within the period valley that have a close companion. In order to do so, we use two numerical approaches: (i) direct  $N$ -body integrations of the equations of motion and (ii) integrations of the orbit averaged secular equations of motion. In both cases we included terms to the equations of motion that account for Schwarzschild precession, apsidal precession due to tidal bulges and terms which account for tidal dissipation.

The direct integrations presented below were performed using ARCHAIN (Mikkola & Merritt 2008). ARCHAIN employs an algorithmically regularized chain structure and the time-transformed leapfrog scheme which allow to integrate the evolution of the motion of arbitrarily tight binaries with arbitrarily mass ratio with extremely high precision. The code includes post-Newtonian (PN) non-dissipative 1PN, 2PN and dissipative 2.5PN corrections to all pair-forces. To these we

also added terms that account for precession induced by tidal bulges as well as tidal dissipation. Velocity-dependent forces were implemented using the generalized mid-point method described in Mikkola & Merritt (2006). The tidal perturbation force was set equal to (Hut 1981)

$$\mathbf{F} = -G \frac{M_* M_1}{r^2} \left\{ 3 \frac{M_*}{M_1} \left( \frac{R}{r} \right)^5 k \left( 1 + 3 \frac{\dot{r}}{r} \tau \right) \hat{r} \right\}, \quad (6)$$

where  $M_1$  is the mass of the planet and  $R$  its radius hereafter set equal to one Jupiter radius,  $k$  (set to 0.28) is the apsidal motion constant and  $\tau$  is the *constant* time-lag factor. Hereafter we use  $M_* = 1M_\odot$ .

The secular integrations performed in this paper make use of the standard octupole level secular equations of motion of Blaes et al. (2002, their Eq. 11-17), including terms accounting for relativistic precession. We added terms that describe apsidal precession induced by tidal bulges and tidal friction. The perturbing acceleration (6) causes a slow change of the orbital parameters. Following Socrates et al. (2012), in the limit of high  $e$ , the orbit



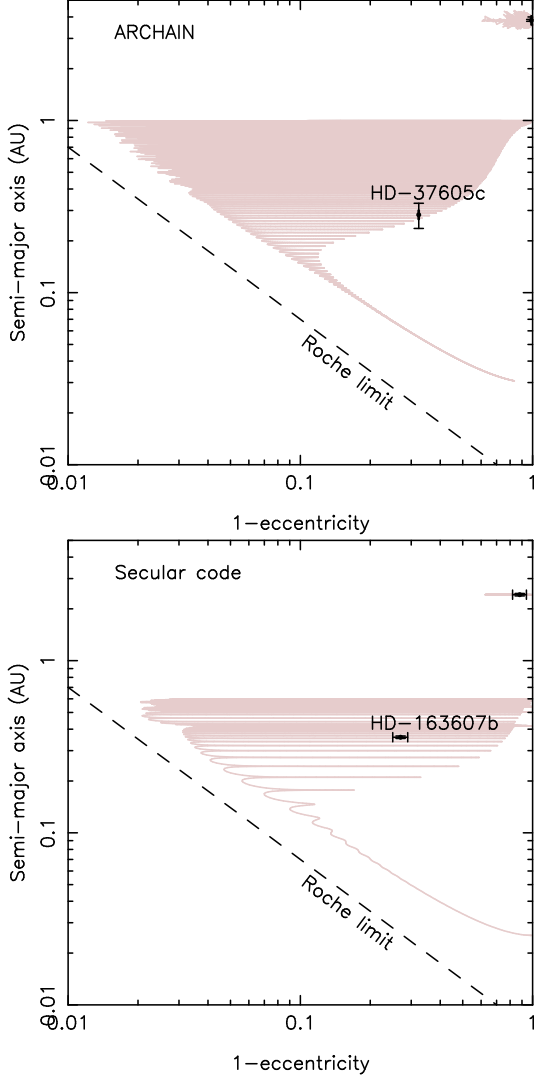


FIG. 2.— Evolution examples that lead to the formation of two planet systems resembling the observed systems HD-37605 and HD-163607. In the lower panel we evolved the system using the secular equations of motion, in the upper panel we used the direct integrator ARCHAIN. Dashed lines indicate the limit below which the planet will undergo Roche-lobe overflow. In both cases the systems are initially stable according to Equation (3). The inner planet evolves to attain an orbit that is consistent with the orbits of the observed planets. These two systems represent therefore possible candidates for a secular migration origin, although our stability analysis suggests that HD-163607b could not have migrated from distances much larger than  $\sim 0.6$  AU.

average change rate corresponding to Equation (6) is

$$\frac{\dot{a}}{a} = -\frac{4059}{320t_D} \sqrt{\frac{a_F}{a}}, \quad (7)$$

$$\frac{\dot{e}}{e} = \frac{\dot{a}}{a} \frac{(1-e^2)}{2e^2}, \quad (8)$$

and

$$\dot{\omega} = \frac{15 [G(M_*)]^{1/2}}{8a_1^{13/2}} \frac{8 + 12e_1^2 + e_1^4}{(1-e_1^2)^5} \frac{M_*}{M_1} kR^5, \quad (9)$$

where  $a_F = a(1-e^2)$ , and  $t_D$  is the characteristic time

for tidal dissipation:

$$t_D = \frac{M_1 a_F^8}{6k\tau GM_*^2 R^5}. \quad (10)$$

In our simulations we neglected any additional precession induced by the stellar host rotational bulge. For the cases considered here we find in fact that the precession due to tidal bulges is dominant and rotational bulges become important only for rapidly rotating stars with spin period less than  $\approx 1$  day. Finally we assume that the inner planet was disrupted by its host star tidal field if it crossed the Roche limit:

$$a_1(1-e_1) \leq 0.01 \frac{R}{R_{\text{Jupiter}}} \left( \frac{M_*}{M_\odot} \frac{M_{\text{Jupiter}}}{M_1} \right)^{1/3} \text{ AU}. \quad (11)$$

The secular integrations base on two two levels of approximation being implemented: (i) double-orbit averaging, (ii) perturbation up octupole-order. More specifically, the orbit average approximation, on which the Blaes et al. (2002) treatment is based on, breaks down if (Antonini et al. 2014):

$$\frac{a_2(1-e_2)}{a_1} \lesssim 0.2 \left( \frac{M_\odot}{M_*} \frac{M_2}{M_{\text{Jupiter}}} \right)^{1/3} \left( \frac{a_1}{a_{\text{cr}}} 0.1 \right)^{1/6}. \quad (12)$$

For values of  $a_2/a_1$  smaller than the one given by this last equation the orbital angular momentum of the inner planet can undergo oscillations on a timescale shorter than its orbital period. Clearly, this condition is never met for the two-planet systems considered here unless the orbits of the planets are crossing. Mean-motion resonances are also neglected in our secular integrations. We note that for  $a_2/a_1 \approx 3$ , their effect might not be fully negligible. The potential associated with  $q$ -th order mean-motion resonances has terms with amplitude  $\sim e^q$  and since the eccentricities are order unity (especially for migrating planets) their effect might be significant. Moreover, even if the effect of mean-motion resonances is negligible, then the octupole-level expansion might not resolve the behavior of the  $N$ -body properly for low  $a_2/a_1$  as more terms in the expansion might be needed. Although we caution on the simplifications implemented in our treatment the results of secular and direct integrations were compared for a number of initial conditions and found to give in general consistent results.

In Figure 2 we show two example cases. The top panel shows a three body integration with initial conditions representing a possible progenitor for HD-37605c and initial mutual inclination  $I = 94^\circ$ . The observed system consists of an eccentric ( $e_1 = 0.68$ ) WJ at  $a_1 = 0.28$  AU and minimum mass  $M_1 \sin i = 2.8 M_{\text{Jupiter}}$ , with a companion at  $a_1 = 3.8$  AU and minimum mass  $M_2 \sin i = 3.4 M_{\text{Jupiter}}$ . Accordingly to our analysis of Section 2, this is the only two planet system hosting a WJ within  $\leq 0.5$  AU that would be dynamically stable if we were to place the inner planet at 1 AU on a highly eccentric orbit. Thus, HD-37605c is a possible candidate for a secular migration origin. The example in the upper panel of Figure 2 shows that this secular migration scenario is indeed a possibility for such a system. The inner planet starts at  $a_1(0) = 1$  AU and evolves to become a HJ. During this transition the inner planet orbital semi-major

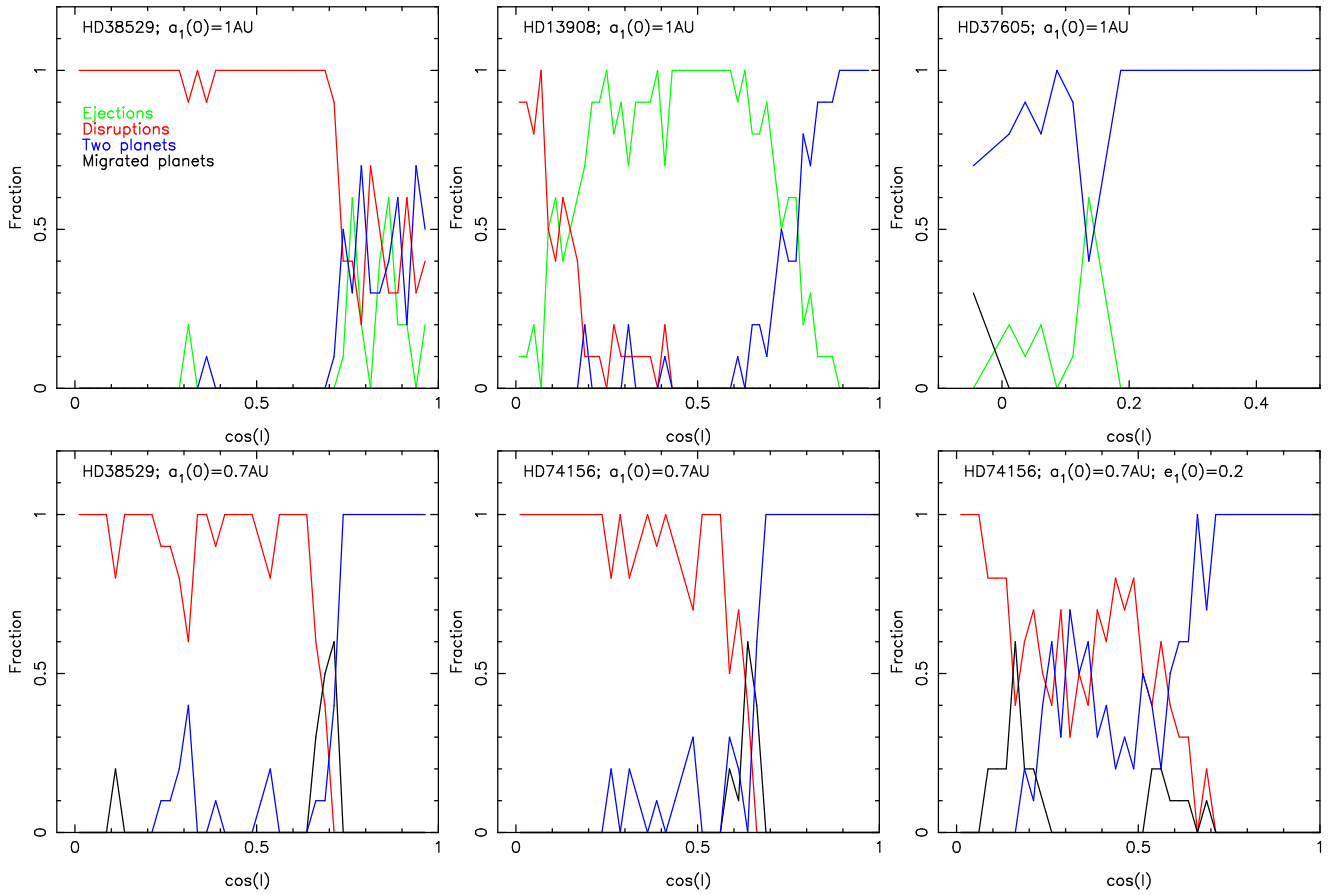


FIG. 3.— Results of the direct  $N$ -body integrations. In the upper panels the inner planet was started at  $a_1(0) = 1\text{AU}$ , while in the lower panels at  $a_1(0) = 0.7\text{AU}$ . The initial values of  $a_2$ ,  $e_2$ ,  $M_2$  and  $M_1$  are given in Table 1 for each system. Here we set the initial masses equal to the minimum mass given in the table. Note that no HJ and WJ is produced for configurations that violate the stability criteria of Section 2. When the initial conditions are stable for large mutual inclinations (bottom panels), LK cycles combined with tidal friction lead to the formation of HJs and WJs. Systems in which one of the two planets is ejected during the simulation are indicated as “Ejections”; Systems in which the inner planet had crossed its Roche limit are indicated as “Disruptions”. “Migrated planets” are systems in which at the end of the simulation the innermost planet was at  $a_1 \leq 0.5\text{AU}$ . Systems that are stable and in which the innermost planet did not experience significant tidal dissipation ( $a_1 > 0.5\text{AU}$ ) are indicated as “Two planets”.

axis and eccentricity take values that are consistent with the observed orbit of HD-37605c. Note that the amount of time the system spends in this region of parameter space depends on the efficiency of tidal dissipation which in turns is regulated by the poorly constrained value of  $\tau$  in Equation (6). However, the characteristic shape of the envelope within which the planet orbit evolves does not depend significantly on the assumed value of  $\tau$  (See also Section 4).

For the bottom panel of Figure 2 we show a secular integration of a two planet system with initial conditions that resemble the observed system HD-163607 and mutual inclination  $I = 84^\circ$ . In this case we start the inner planet at  $a_1(0) = 0.6\text{AU}$ . The observed system consists of an eccentric ( $e_1 = 0.73$ ) WJ at  $a_1 = 0.36\text{AU}$  and minimum mass  $M_1 \sin i = 0.77M_{\text{Jupiter}}$ , with a companion at  $a_1 = 2.4\text{AU}$  and minimum mass  $M_2 \sin i = 2.3M_{\text{Jupiter}}$ . Even in this case the inner planet evolves through a region of parameter space which is consistent with the observed orbit of the planet HD-163607b.

#### 4. $N$ -BODY SIMULATIONS: NEAR THE EDGE OF STABILITY

In this section we consider the evolution of 2 planet systems that are close to the stability boundary defined

by Equation (3). In particular we focus on systems with properties that resemble those of the two planet systems HD-38529, HD-74156 and HD-13908. (We specifically analyzed the stability of these three systems because their value of  $r_{\text{cr}}$  in Table 1 is just below 1AU. Thus, given the uncertainty in the adopted stability criteria, it is unclear whether these systems will be actually unstable at  $a_1 \approx 1\text{AU}$ .) The results of these simulations are used to validate the stability criteria adopted above and our argument that systems which are dynamically unstable according to these criteria do not lead to tidal migration but rather to planet ejections and collisions with the stellar host.

We run 1200 direct integrations, 200 per panel in Figure 3. The initial mutual inclination between the inner and outer planet orbits,  $\cos(I)$ , was sampled uniformly between 0 and 1. The initial inner and outer planet argument of periapsis  $\omega_1$  and  $\omega_2$  and the longitude of the ascending nodes  $\Omega_1$  and  $\Omega_2$  were chosen randomly between 0 and  $2\pi$ . The outer planet initial eccentricity and semi-major axis were set equal to the observed values while the inner planet eccentricity was initially set to a fixed value (0.01 and 0.2). We take the mass of the planets to be equal to the minimum mass as inferred from observations. We set  $\tau = 66\text{sec}$ , and evolved each system for a

maximum time of  $10^8$ yr. In addition we run ten retrograde configurations,  $\cos(I)$  in the range  $(-0.1 - 0)$ , for initial conditions corresponding to HD37605. By comparing a number of orbit-average integrations in which we adopted different values of  $\tau$ , we found that the results of these integrations can be rescaled using

$$t' \rightarrow t \times \frac{\tau}{\tau'}, \quad (13)$$

so that evolving a system for  $10^8$ yr with  $\tau = 66$ sec would be at a good approximation equivalent to evolve the same system for  $10^{10}$ yr with  $\tau = 0.66$ sec. This latter value of  $\tau$  is large enough to allow the formation of HJs at  $\lesssim 0.1$ AU in  $10^{10}$ yr (Socrates et al. 2012). We caution that although the scaling of Equation (13) is almost exact for stable systems, it might be an oversimplification near the region of instability given that our direct simulations cannot identify whether a system will be unstable on timescales longer than  $10^8$ yr. In addition to this, the outer planet mass could be larger than the adopted value which will render the system even more susceptible to dynamical instabilities. It is likely therefore that in our analysis we are overestimating the number of stable systems.

Figure 3 displays the results of the direct integrations. In the upper panels the inner planet semi-major axis is initially  $a_1(0) = 1$ AU. In these cases most configurations are unstable leading to planet disruptions (red curves) or ejection of one of the planets (green curves). We also checked for any collision between the two planets but did not find any. We calculate the number of “migrated” planets as those that have reached within  $a_1 \leq 0.5$ AU at the end of the integration. As expected, for configurations that are unstable according to Equation (3) no migrating planet was formed. Three planets had  $a_1 \leq 0.5$ AU for the initial conditions corresponding to HD37605c, however, only for retrograde configurations. This is a consequence of the back-reaction torque of the inner planet on the outer orbit which shifts the initial critical inclination at which the maximum possible  $e$  is attained at  $\geq 90^\circ$ . Note that a more massive perturber will reduce this effect and allow the formation of WJs and HJs also for prograde configurations.

In the bottom panel of Figure 3 we set  $a_1(0) = 0.7$ AU. These configurations are stable according to our stability criteria, although they are near the extreme of inequality (5). At large inclinations,  $\cos(I) \lesssim 0.5$ , the inner planet orbit becomes extremely eccentric so that in most cases the planet collides with the star. This is expected since in all cases considered here the maximum eccentricity attained by the inner planet is not limited by precession due to tidal bulges which becomes a limiting factor for the maximum  $e_1$  only at  $a_2/a_1 \gtrsim 4$ . Nevertheless, a few planets managed to migrate within 0.5AU for a mutual inclination that lies initially near or above the LK critical angle,  $\cos(I) \approx 0.65$ . In these cases, the inner planets attain an eccentricity that is large enough to allow for efficient tidal dissipation, but, due to the mild initial inclinations, never high enough to cause the disruption of the planet. For initial inclinations smaller than  $\cos(I) \approx 0.65$ , the inner planet eccentricity cannot be excited to high values so that the system is more stable and the orbital parameters of the planets remain essentially unchanged during the evolution.

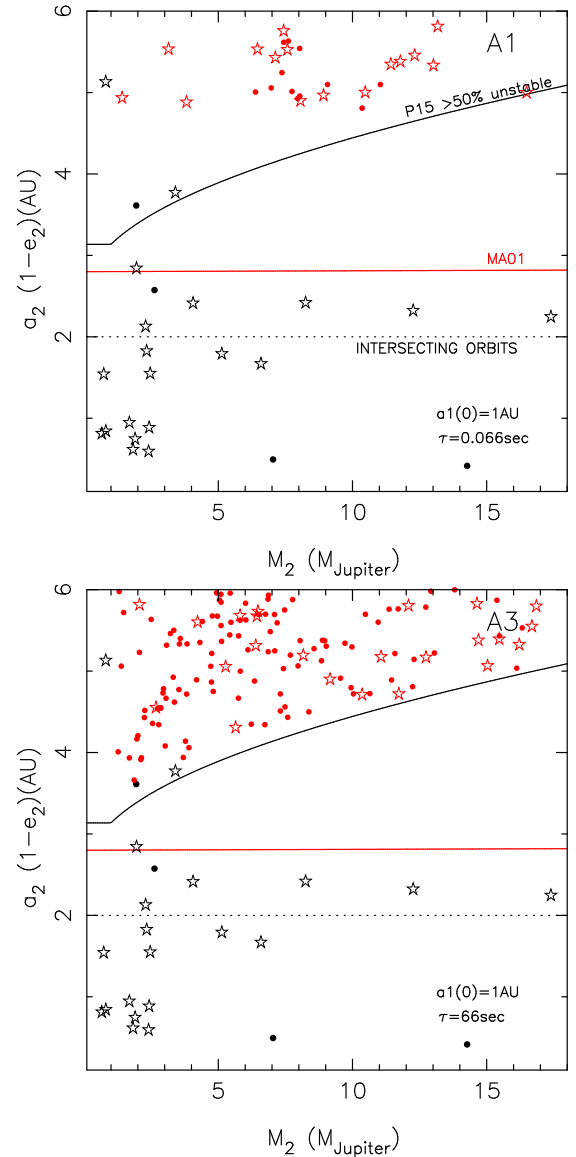


FIG. 4.— Solid lines show regions of stability. Any proto-HJ/WJ with  $a_1 = 1$ AU,  $e_1 = 1$ , and  $M \sin I \geq 0.5 M_{\text{Jupiter}}$  would be unstable according to Equation (5) if its external companion lay below the horizontal red line (labelled MA01). The other solid line corresponds to Equation (3). Below the dashed line the two planets would be on intersecting orbits. Simulations results are shown for models A1 and A3 (see Table 2). Red stars indicate WJs, i.e., those systems in which the inner planet has experienced significant tidal dissipation and migrated within 0.9AU but has not evolved inside 0.1AU. Red points are systems that have formed a HJ ( $a_1 < 0.1$ AU) at the end of the integration. Black symbols correspond to the observed systems of Table 1. Black stars are WJs ( $a_1 = 0.1 - 1$ AU); black points are HJs ( $a_1 < 0.1$ AU).

In conclusion, our direct integrations show that LK induced migration is unlikely to occur for unstable systems while it can lead to the formation of hot and warm Jupiters for systems that are just below the stability boundaries, although, as shown next, these are likely to be rare.

## 5. ORBIT AVERAGE TREATMENT: MIGRATING PLANETS AND THEIR ORBITAL DISTRIBUTION

In this Section we run suites of LK simulations, in which systems are initialized with two Jupiter mass planets at high mutual inclination. By comparing the

TABLE 2  
RESULTS OF SECULAR INTEGRATIONS

Model	Stability criterion	$a_1(0)$ (AU)	$e_1(0)$	$e_2(0)$	$\tau$ (sec)	HJs %	WJs %	Non-migrating %	Disrupted %
A1	P15	1AU	0.1	0.2	0.066	0.77	1.02	70.7	27.5
A2	-	1AU	0.1	0.2	0.66	1.22	0.90	64.4	33.5
A3	-	1AU	0.1	0.2	66	10.3	1.54	59.3	28.9
B1	-	0.6AU	0.1	0.2	0.066	1.73	0.70	66.4	31.2
B2	-	0.6AU	0.1	0.2	0.66	4.41	0.51	65.1	29.9
B3	-	0.6AU	0.1	0.2	66	21.8	0.83	56.9	20.5
C1	MA01	0.6AU	Rayleigh	Rayleigh	0.066	3.01	0.32	68.5	28.2
C2	-	0.6AU	Rayleigh	Rayleigh	0.66	4.73	1.09	67.1	27.1
C3	-	0.6AU	Rayleigh	Rayleigh	66	19.7	2.05	60.4	17.9
C1-c	-	0.6AU	Rayleigh	Rayleigh	0.066	1.86	0.58	79.0	18.6
C2-c	-	0.6AU	Rayleigh	Rayleigh	0.66	4.41	0.96	74.3	20.3
C3-c	-	0.6AU	Rayleigh	Rayleigh	66	16.1	1.73	67.2	15.0

We define here as HJs those planets that by the end of the simulation have migrated within 0.1AU; WJs are defined as those planets that are in the semi-major axis range  $0.1 - 0.9\text{AU}$  (for  $a_1(0) = 1\text{AU}$ ) or  $0.1 - 0.5\text{AU}$  (for  $a_1(0) = 0.6\text{AU}$ ). Non-migrating planets have final semi-major axis  $a_1 \geq 0.9\text{AU}$  (for  $a_1(0) = 1\text{AU}$ ) or  $a_1 \geq 0.5\text{AU}$  (for  $a_1(0) = 0.6\text{AU}$ ); “disrupted” systems are those in which the inner planet had crossed its Roche limit. In the first models we run the integrations up to a maximum time of 10Gyr. In the last three models (C1-c, C2-c, C3-c) the final integration time was chosen randomly between 0 and 10Gyr. This latter choice is to simulate a scenario in which the planets have formed continuously over the last 10Gyr. In order to account for the fact that we have only selected systems with an inclination  $50^\circ$ , we have reduced the number of forming HJs and WJs (and disrupted) by  $\cos 50^\circ$ , and then used that number in the fraction.

ratio of WJs to cold Jupiters (CJs) found in the simulations to that ratio as observed we put constraints on the fraction of observed WJs that are likely to have undergone high- $e$  LK migration.

In our simulations we set the mass of the inner planet to  $M_1 = 1 M_{\text{Jupiter}}$  and sample the mass of the outer perturber uniformly in the range  $1 \leq M_2 \leq 17 M_{\text{Jupiter}}$ . These latter values correspond approximately to the extremes of the mass distribution of the observed Jupiter companions to HJs and WJs. We assume the orbits to be prograde and sample the mutual inclination from a uniform distribution in  $\cos(I)$ . We take the mutual inclination in the range 50 to 90 degrees. The high mutual orbital inclination is required in order for the inner planet to reach high eccentricities. We adopt a small initial eccentricity for the inner planet  $e_1 = 0.1$  and take  $e_2 = 0.2$  for the outer planet. This latter value is close to the median of the eccentricity distribution for the outer companion of observed HJs and WJs. The outer planet semi-major axis is sampled uniformly within  $a_2 \leq 8\text{AU}$  with the lower limit set such that the system satisfied the stability condition of Equation (3) in the limit  $e \rightarrow 1$ . We considered two values of the inner planet semi-major axis:  $a_1 = 1\text{AU}$ ,  $a_1 = 0.6\text{AU}$ . For each value of  $a_1$  we considered three values of the time-lag constant  $\tau = 0.066$ ,  $0.66$  and  $\tau = 66\text{sec}$ , which correspond to a tidal quality factor  $Q$  of  $\approx 10^6$ ,  $10^5$  and  $10^3$  respectively. Thus, we evolved 6 sets of initial conditions. For each set we performed a total of 1000 random realizations integrating them up to a final integration time of 10Gyr.

In addition to the secular integrations described above we run 3 sets of initial conditions (corresponding to the three values of  $\tau$ ) where we used a Rayleigh distribution for both  $e_1$  and  $e_2$  with a mean eccentricity of 0.175 (Moorhead et al. 2011), and this time sampling  $a_2$  such that the system satisfied the stability condition of Equation (5). In these latter simulations (models C in Table 2), the planets can have initially a lower  $a_2/a_1$  ratio which favors the formation of WJs as discussed in Section 2. As a consequence of this, such models are expected to

produce more WJs than if we were to select the initial conditions based on inequality (3), however we caution that they also contain more systems that are near the orbit crossing when  $e_1 \approx 1$  and for which the orbit-averaged treatment we use is less accurate.

Table 2 gives the initial setup of the numerical integrations and summarizes the main results of our simulations, giving the fraction of systems that lead to the specified outcomes. In order to take into account the fact that we are only simulating systems with mutual inclinations larger than  $50^\circ$  we reduced the number of forming HJs and WJs (and disrupted) by  $\cos 50^\circ$ , and then used that number in the fraction. We find that a high- $e$  LK migration scenario is more efficient at producing HJs than WJs. The fraction of systems that result in the formation of WJs is  $\approx 1\%$  of the total and it is roughly constant, having little variation with the initial conditions and tidal dissipation strength. The fact that the number of  $WJs$  is not very sensitive to  $\tau$  is because increasing  $\tau$  will result in a larger number of planets migrating inside the period valley, but at the same time also in a larger number of planets leaving it. According to our results, if WJs are migrating planets, then for a homogeneous sample of planets we would expect that planets with detected outer companions would more often be HJs than WJs. This expectation appears to be at odds with what is observed. Restricting our analysis to the subset of known extrasolar planets discovered by radial-velocity surveys, only 2 of the Jupiter mass planets ( $M_1 \sin i \geq 0.5 M_{\text{Jupiter}}$ ) at  $\leq 0.1 \text{AU}$  have a detected outer companion within  $\lesssim 5\text{AU}$  distance from their host star, while 20 Jupiters mass planets at  $0.1\text{AU} \leq a_1 \leq 1 \text{AU}$  do. This suggests that HJs and WJs belong to two distinct populations of planets which likely originated through different processes.

Figure 4 shows the properties of outer companions to the observed HJs (black points) and WJs (black stars). The black and red curves show the value of  $a_2$  satisfying the condition Equations (3) and (5) respectively. Below these lines WJs are unlikely to form as the system is



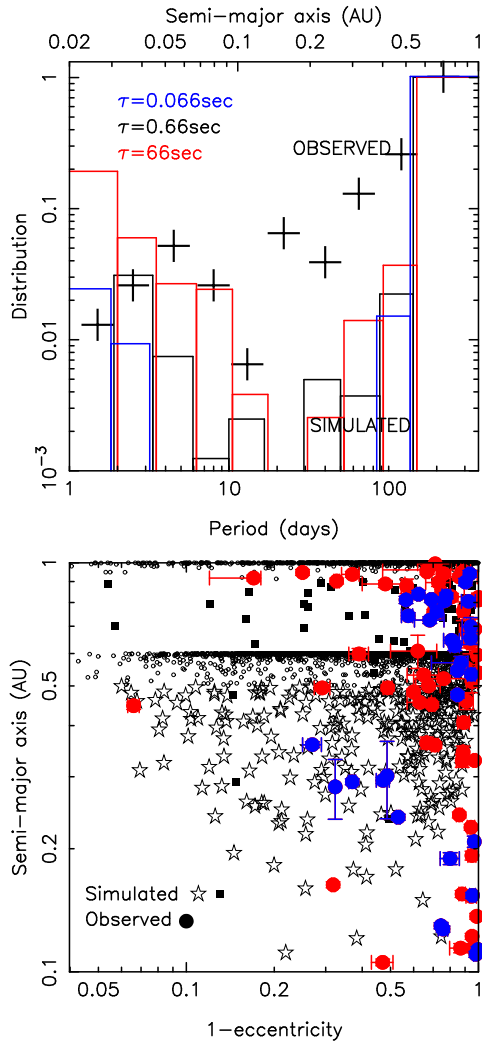


FIG. 5.— Upper panel: semi-major axis distribution of the planets from our simulations (histogram) compared to the observed distribution from Santerne et al. (2015) (crossed symbols). The simulated distributions are from the C1-c, C2-c and C3-c models that have  $a_1(0) = 0.6\text{AU}$  (see Table 2). Other models that have  $a_1(0) = 0.6\text{AU}$  were found to produce similar distributions. The observed and simulated distributions have been normalized such to have the same value at periods  $P \gtrsim 200\text{days}$ . Note how any of our models greatly underestimates the number of Jupiters in the WJ zone. Lower panel:  $a$  vs  $e$  distribution of the inner planets for systems that were evolved forward in time using the secular equations of motion. Small open circles are systems that have not experienced significant inward migration. Filled square symbols (star symbols) correspond to planets with  $a_1(0) = 1\text{AU}$  ( $a_1(0) = 0.6\text{AU}$ ) and that migrated within  $0.9\text{AU}$  ( $0.5\text{AU}$ ) by the end of the simulation. Note that models with  $a_1(0) = 1\text{AU}$  produce almost no WJs inside  $0.5\text{AU}$ . These distributions are compared to observational data which are represented by the filled circles. Data points corresponding to Jupiters with a known Jupiter companion are in blue. In the lower panel data are from exoplanets.org.

unstable to either collision or ejection of one of the planets. As done previously in Section 2 we computed the stability limit from Equations (3) by taking the relevant limit  $e_1 \rightarrow 1$ . In Figure 4 the relative position of the black points to the stability lines show that only four of the twenty-four observed systems would be dynamically stable if the inner planet had  $a_1 = 1\text{AU}$ , and fourteen of them would be on intersecting orbits. Figure 4 also displays the results from models A1 and A3 of Table 2, showing the systems that form HJs (red points) and those

that form WJs (red stars). These latter being defined as those systems in which the innermost planet had experienced significant tidal dissipation and migrated inside the semi-major axis range  $0.1 - 0.9\text{AU}$ . From this figure we see again that the number of migrated planets that have formed a HJ increases significantly when increasing the time-lag factor  $\tau$ , while the number of migrating planets in the period valley (red stars) increases but only slightly. Accordingly, the number of HJs formed in our models is typically equal or larger than the number of migrating WJs.

In the upper panel of Figure 5 we show the period distribution of migrating planets and compared this to the (intrinsic) observed distribution from Santerne et al. (2015). Such comparison shows that the semi-major axis distribution of the planets in our simulations does not provide a good match to the observed period distribution of gas giants in the period valley. Given the observed number of Jupiters at  $P \gtrsim 100\text{days}$ , the models underpredict the number of migrating planets below this period by at least one order of magnitude. We conclude that a high- $e$  migration mechanism can be responsible for less than 10% of all gas giants with orbital periods in the range  $10 - 100\text{days}$ .

We note that our simulations are restricted to systems with inner planets initially at  $\leq 1\text{AU}$ , accompanied by an outer perturber within  $\leq 8\text{AU}$ . A significant contribution to the WJ population from planets migrating from  $\gg 1\text{AU}$  and having companions at  $\gg 8\text{AU}$  is unlikely. In fact, as also noted in Section 2, WJs cannot form for Jupiter mass perturbers if  $a_2$  is larger than a few AUs.

Finally, we note that similar to previous studies (e.g., Anderson et al. 2015), our model distributions do not match the period distribution of HJs ( $< 10\text{d}$ ), producing too many planets at short orbital periods ( $\sim 1\text{d}$ ). Such discrepancy might depend on the choice we made for various parameters, most importantly on the adopted value of the planet radius which determines the final semi-major axis of the HJ (Wu & Lithwick 2011).

A secular migration model for WJs fails at explaining some additional features of the observed orbital distribution. First, in only three of the 3000 models that were started at  $a_1(0) = 1\text{AU}$  the inner planet was found in the region  $0.1 - 0.5\text{AU}$  by the end of the simulation. This is in contrast with the abundance of observed Jovian planets at these radii and casts further doubts on a possible migratory origin from  $\gtrsim 1\text{AU}$  for these systems. If the planets started with a smaller semi-major axis  $a_1(0) = 0.6\text{AU}$ , as shown in Figure 5 then for each Jupiter in the radial range  $0.1 - 0.5\text{AU}$  our models produce at least ten more (mostly non-migrating) Jupiters within the range  $0.5 - 1\text{AU}$ . Contrary to this, observations yield roughly the same number of giant planets in these two ranges of semi-major axes.

The lower panel of Figure 5 shows the final  $a$  vs  $e$  distribution of the simulated systems compared to the observed distribution. This plot shows an additional important feature of the simulated distribution which is difficult to reconcile with observations: the lack of low- $e$  WJs at  $a_1 \lesssim 0.3\text{AU}$ . In fact, none of our models produced a WJ with  $e \lesssim 0.3$  at these radii, while  $\sim 80\%$  of known planets with semi-major axis  $0.25 \leq a_1 \leq 0.1$  have eccentricities  $\lesssim 0.3$ . Evidently giant planets observed in this region of parameter space are unlikely to have formed

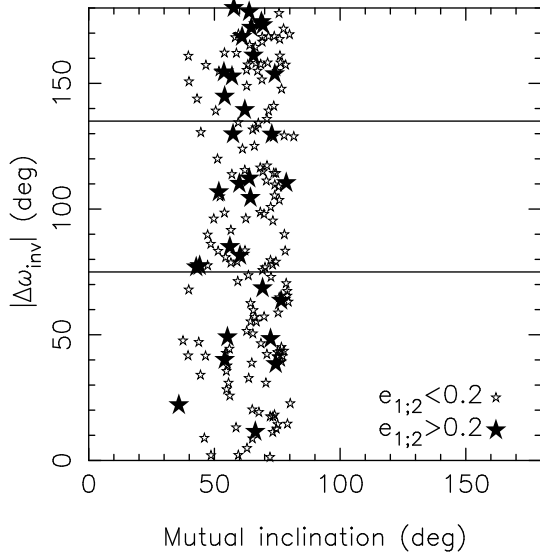


FIG. 6.— Difference in apsidal longitudes,  $\Delta\omega_{\text{inv}} = \omega_1 - \omega_2$ , as a function of mutual inclination for the WJs formed in our secular integrations. Filled-star symbols are the sub-set of systems comprising an eccentric WJ with eccentric outer companion.  $e_1$  and  $e_2$  are the final value of the eccentricity of inner and outer planets, i.e. those at the time at which the apsidal longitudes were computed.

through secular migration induced by an outer perturber planet. This latter point is further discussed in the next section.

Dawson & Chiang (2014) showed that eccentric WJs with eccentric outer giant companions have apsidal separations which cluster near  $90^\circ$ . Dawson & Chiang (2014) interpreted this as signature of mutual inclinations being between  $35 - 65^\circ$ , favoring LK migration as the mechanism for the formation of the inner planets. In Figure 6 we show the distribution of the apsidal misalignment,  $\Delta\omega_{\text{inv}} = \omega_1 - \omega_2$ , as a function of mutual inclination for the migrating WJs in our secular integrations. Interestingly, our simulated planets do not show any significant clustering around  $\Delta\omega_{\text{inv}} = 90^\circ$ . The WJs formed in our models have mutual inclinations in the range  $40 - 80^\circ$ , but their  $\Delta\omega_{\text{inv}}$  appear to be uniformly distributed. These results suggest some other process, other than LK oscillations, as responsible for the near orthogonality of apsides exhibited by the observed WJs.

### 5.1. Evolution towards low semi-major axes

As shown in Figure 5 a high- $e$  LK migration scenario for WJs fails at producing systems with a low value of  $a$  and  $e$  that are indeed quite numerous among the observed systems. In fact none of our simulations produced a system in the region where, for example, HD-38529b and HD-13908b are observed ( $0.1 - 0.3\text{AU}$ ), disfavoring a LK induced migration scenario for the formation of these planets. As discussed below, the reason for this is the reduced range of eccentricity oscillations due to Schwarzschild precession as the planet semi-major axis shrinks due to tidal dissipation.

At the quadrupole order level and in the test particle limit the quantity

$$H = \ell^2 + \sin^2 I (\ell^2 + 5e_1^2 \sin^2 \omega) - \frac{k}{\ell}, \quad (14)$$

with  $\ell = \sqrt{1 - e_1^2}$ , is an integral of motion as it differs

from the system Hamiltonian only by a constant (e.g., Merritt 2013). The third term in the right hand side of Equation (14) represents the extra Schwarzschild precession term where

$$k = 8 \frac{M_\star}{M_2} \frac{r_g a_2^3}{a_1^4} (1 - e_2^2)^{3/2}, \quad (15)$$

and  $r_g = GM_\star/c^2$ .

From the conservation of  $H$  and  $\ell_z = \ell \cos I$  we can derive a relation between the maximum ( $\ell_+$ ) and minimum ( $\ell_-$ ) angular momentum attained during a LK oscillation for a given value of  $\ell_z$ . When the argument of periapsis  $\omega$  librates around  $\pi/2$  the maximum and minimum values of  $\ell$  are related through the equation:

$$\ell_+^2 \ell_-^2 = \frac{5}{3} \ell_z^2 + \frac{k}{3} \left( \frac{\ell_+ - \ell_-}{\ell_+^2 - \ell_-^2} \right) \ell_+ \ell_-. \quad (16)$$

As the planet semi-major axis decreases due to tidal dissipation, relativistic precession will increase the portion of parameter space available for circulation at expenses of libration, gradually pushing an initially librating orbit toward the separatrix at which  $\ell_+ = 1$ , and finally onto a circulating orbit (see also Blaes et al. 2002; Anderson et al. 2015, for a similar analysis).

The distance at which the fixed point does not longer exist is found by setting  $\omega = \pi/2$  and  $\dot{\omega} = 0$ , which yields:

$$\tilde{a} = \left[ 4 \frac{M_\star}{M_2} \frac{r_g a_2^3 (1 - e_2^2)^{3/2}}{3 - 5\ell_z^2} \right]^{1/4} \approx 0.2 \left( \frac{M_\star}{M_\odot} \right)^{1/2} \left( \frac{M_2}{M_{\text{Jupiter}}} \right)^{-1/4} \left( \frac{a_2 \sqrt{1 - e_2^2}}{3\text{AU}} \right)^{3/4} \left( \frac{2a_1}{a_1 - a_{\text{cr}}} \right)^{1/4} \text{AU}, \quad (17)$$

where we have used the fact that  $\ell_z \approx \sqrt{3/5} \ell_-$  (from  $\ell_z = \cos(I)\ell$  and  $\cos(I) \approx \sqrt{3/5}$  at  $\ell_-$ ) and set  $\ell_- = a_{\text{cr}}/a_1$  as required for efficient tidal dissipation to occur. Below  $\tilde{a}$  librating solutions do not longer exist.

After  $\omega$  starts circulating  $\omega = \pi/2$  at  $\ell = \ell_-$  and  $\omega = 0$  at  $\ell = \ell_+$ , which leads to the relation

$$\ell_+^2 = \frac{5}{2} \left( 1 + \ell_z^2 - \frac{3}{5} \ell_-^2 - \frac{\ell_z^2}{\ell_-^2} \right) + \frac{k}{2} \left( \frac{1}{\ell_+} - \frac{1}{\ell_-} \right). \quad (18)$$

According to Equation (18) and for  $a_1 < \tilde{a}$ ,  $\ell_+$  must become smaller as  $a_1$  decreases, thereby pushing the planet away from the region of small  $a_1$  and  $e_1$ .

A good approximation to Equation (18) can be obtained by noting that  $\ell_z \approx \sqrt{3/5} \ell_-$  and  $k/\ell_+ \approx k$  (from  $\ell_+ \approx 1$ ), which leads to the simpler relation

$$\ell_+^2 \approx 1 + \frac{k}{2} \left( 1 - \frac{1}{\ell_-} \right), \quad (19)$$

for circulating orbits. Although quite simplified and reasonable only for an orbit close to the separatrix, Equation (19) was found to reproduce the results of numerical simulations fairly well. A few example systems are shown in Figure 7. The dashed curve in the figures that demarcate the  $\ell_-$  envelope is a curve of constant angular momentum:  $\sqrt{a_1} \ell$ .  $\ell_-$  tracks this curves because tidal dissipation occurs mostly at  $\ell = \ell_-$ . In the upper left panel the inner planet argument of periapsis is

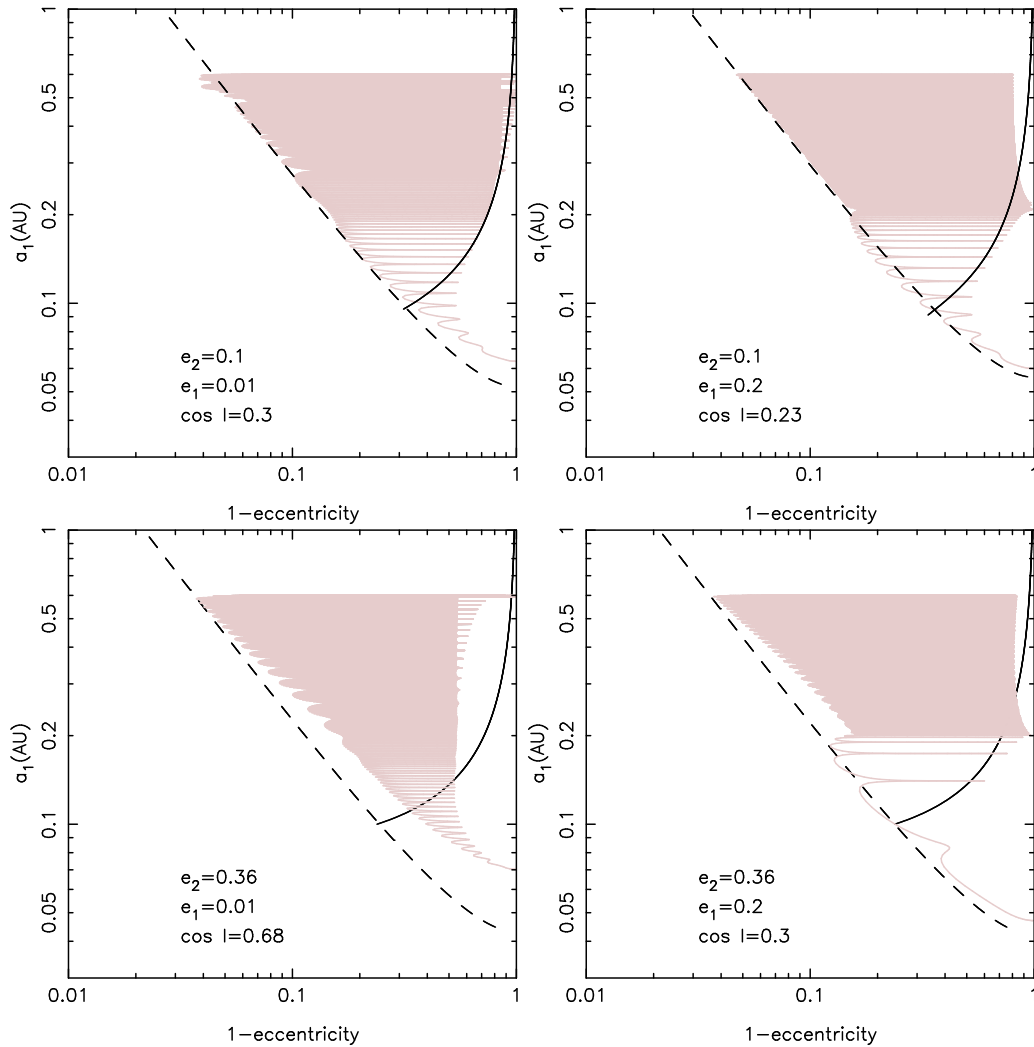


FIG. 7.— Orbital evolution of migrating planets obtained with the secular equations of motion. The solid lines give the minimum eccentricity attained during the LK oscillations as predicted by Equation (19); dashed lines are lines of constant angular momentum which give the value of  $\ell_-$  we have used to compute the solid line. In the lower panels the eccentricity of the outer planet is  $e_2 = 0.36$ , which causes the octupole order terms to become important to the evolution. In all panels the inner planet argument of periapsis was set to  $\omega_1 = \pi/2$  and the mass of the outer planet was  $17M_{\text{Jupiter}}$ ;  $\omega_2$  was set equal to (in radians) 3 (upper left), 0.013 (upper right and lower left) and 2.6 (lower right).

initially circulating and the  $\ell_+$  value steadily decreases with time. In the upper right panel instead  $\omega$  is initially librating. From Equation (16) we see that the inclusion of the extra Schwarzschild precession term will tend to increase  $\ell_+$  as the orbit shrinks. Accordingly, from Figure 7 we see that as the orbit decays  $\ell_+$  increases until it crosses the separatrix at  $a_1 \approx 0.2\text{AU}$  where  $\ell_+ \approx 1$ . Then the  $\ell_+$  envelope is set by the separatrix, as modified by Schwarzschild precession and it is approximately equal to the value given by Equation (19) after  $\omega$  starts circulating.

#### 5.1.1. Effect of octupole order terms

If the orbit of the outer planet has a substantial eccentricity (typically  $\gtrsim 0.1$ ), then the octupole order terms can cause the evolution of the inner planet orbit to deviate significantly from the simple model depicted above. However, the distribution shown in Figure 5, which was obtained with the octupole secular code, suggests that even when higher order terms are included the innermost planet orbit keeps away from the region  $a_1 \lesssim 0.3\text{AU}$ ,

$e_1 \lesssim 0.3$ , for  $a_2 \geq 0.6\text{AU}$ .

The octupole order terms have two main effects: (i) the high eccentricity part of the envelope can deviate significantly from a line of constant angular momentum (e.g., lower panels of Figure 7); (ii) if the inner planet argument of periapsis is initially librating, as the semi-major axis decreases due to tidal friction the orbit eventually crosses the LK separatrix where dynamical chaos can drive the orbital eccentricity to very high values. When this happens the planet orbit will tend to “freeze” at higher values of  $e$  so that a HJ will promptly form (see the bottom right panel of Figure 7).

#### 5.2. Multi-planet systems and secular chaos

As mentioned before, another method to excite eccentricities is via secular chaos in multi-planet systems (Wu & Lithwick 2011). Here we show that the conclusions drawn in this section likely applies to such type of systems as well.

In systems that host more than two giant planets, the planets need not be close companions, and need not be

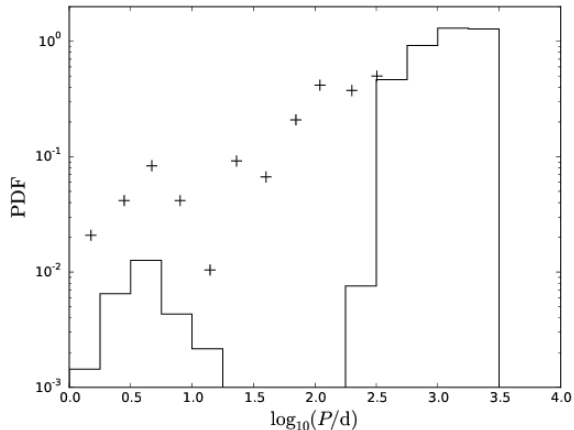


FIG. 8.— Period distributions from secular calculations of high- $e$  migrations in multi-planet systems, with 3 to 5 planets (Hamers et al. in prep). Crossed symbols show the observational data from Santerne et al. (2015), normalized to match the simulated distribution at  $\log_{10}(P/d) \approx 2.6$ .

initially highly eccentric and/or inclined to excite the innermost planet eccentricity to high values, and potentially produce a WJ (e.g., Hamers et al. 2015). However, population synthesis studies with plausible assumptions (Hamers et al. in prep., Antonini et al. in prep.) find that almost no WJs are produced, whereas HJs are produced in more significant numbers (up to a few per cent).

In Figure 8 we show the period distribution of a large set of multi-planet system integrations based on the orbit-averaged code described in Hamers & Portegies Zwart (2015). In these secular simulations, the number of planets was chosen between 3 and 5, and the semi-major axes were sampled linearly between 1-4, 6-10, 15-30, 45-50 and 60-100 AU for the 3 to 5 planets, respectively. The stellar mass was set to  $1 M_{\odot}$ , and the planetary masses were sampled randomly between 0.5 and  $5 M_{\text{Jupiter}}$ . The arguments of periastris and longitudes of the ascending nodes were sampled randomly. The apsidal motion constant was set to 0.28. The time-lag constant was set to  $\tau = 66\text{sec}$ , and the innermost planet radius was to either 1 or  $1.5 R_{\text{Jupiter}}$ ; The inclinations and eccentricities (in units of radians) were sampled from a Rayleigh distribution with an rms width of either 10 or 15 degrees ( $\approx 0.18$  or  $\approx 0.35$  radians).

In total we integrated 10000 systems up to a maximum integration time of 10 Gyr. In our analysis we rejected all systems in which the planet orbits crossed during the integration or in which the inner planet collided with the star. We also tried different values of  $\tau$  ( $= 0.66$ , and  $0.066\text{sec}$ ) but found this not to affect our conclusion: similar to the results of the two-planet system integrations described above, and in stark contrast with the observations, a small number of WJs is produced compared to HJs. Indeed our multi-planet simulations produce essentially no Jupiter in the period valley as can be seen in Figure 8. We conclude that these models as well, greatly underpredict the number of giant planets observed in the period valley.

## 6. ECCENTRICITY DISTRIBUTION

Figure 9 compares the eccentricity distribution of our simulated systems to the distribution of observed WJs.

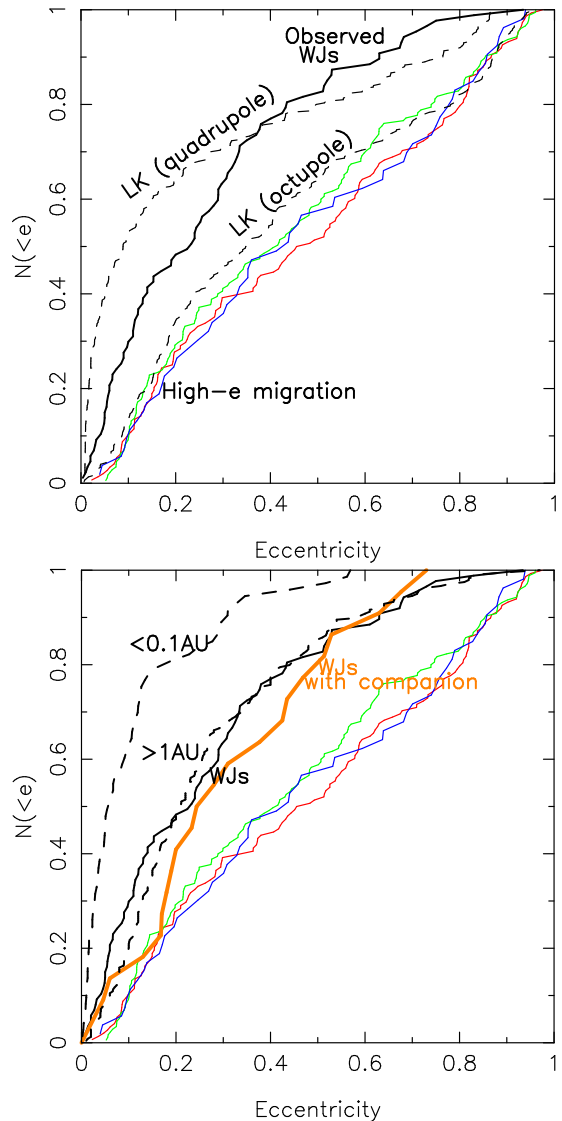


FIG. 9.— Cumulative eccentricity distribution of migrating planets from our two-planets simulations (green, red and blue lines) compared to the observed eccentricity distribution of WJs (black solid lines). All the high- $e$  migration models produce an eccentricity distribution which is significantly different from the observed distribution. In the top panel the dashed curves give the eccentricity distribution of a planet undergoing LK oscillations computed using the secular equations of motion and at the quadrupole (upper curve) and octupole (lower curve) level of approximation. In the bottom panels the black dashed curves are the eccentricity distributions of observed Jupiters in the indicated range of semi-major axes. Orange solid line is for the sub-sample of WJs with one outer companion. The model predictions do not take into account eccentricity-dependent selection effects which might become important at  $e \gtrsim 0.8$ .

The simulated models yield an eccentricity distribution for the migrating planets which is nearly uniform ( $N(<e) \sim e$ ). A comparison of these two populations show that our migration models produce too many highly eccentric WJs to be consistent with observations. The oscillations required to produce inward migration result in more eccentric planets than observed so that the simulated distribution for the migrating population is inconsistent with the observed eccentricity distribution (see also Dawson et al. 2015; Frewen & Hansen 2016). The discrepancy of the migration model with observations is



therefore due to the significant fraction of migrating WJs with high eccentricity, while only a few observed WJs are on high eccentricity orbits (see Figure 5). In fact, as also noted above, a large number of WJs have an eccentricity that is close to zero.

In Figure 9 we show the model eccentricity distributions starting from different initial conditions (models A3, B3 and C3-c in Table 2). These models all produce a similar final eccentricity distribution demonstrating that our conclusions are quite robust and do not depend significantly on the choice we made for the initial conditions. Using the Kolmogorov-Smirnov (K-S) test gives  $p$ -values in the range  $10^{-3} - 10^{-4}$ , indicating that the synthetic and observed  $e$ -distributions are unlikely to be drawn from the same population.

The dashed curves in the top panel of Figure 5 give the eccentricity distribution of a planet undergoing LK oscillations that we computed using the secular equations of motion at the quadrupole (upper curve) and octupole (lower curve) level of approximation. The planet was placed at  $a_1(0) = 0.5\text{AU}$  with a negligible initial eccentricity ( $e_1(0) = 0.01$ ). The outer planet had a mass of  $5M_{\text{Jupiter}}$  and was placed at  $a_2 = 6\text{AU}$  with  $e_2(0) = 0.2$ . The mutual inclination was set to  $70^\circ$ . At the quadrupole level of approximation we can simply derive the eccentricity distribution as  $dN/de = dt/de \sim 1/e_1$  so that  $N \sim \ln e$  – this follows from the fact that in a mixed ensemble the number of planets  $\Delta N$  in the interval  $e \sim e + \Delta e$  is proportional to  $\Delta t$ . As expected, this form matches quite well the eccentricity distribution given by the upper dashed curve in Figure 5, but does not provide a good match to either the observed eccentricity distribution or to the model distribution. The distribution of the migrating Jupiters in our two-planet simulations is instead similar to that of a population of planets undergoing LK oscillations with a non-negligible contribution from the octupole potential (lower dashed curve). We conclude that the dynamical evolution of the planets in our simulations is significantly affected by the octupole order terms. The main effect of the octupole order terms is to skew the eccentricity distribution of WJs towards higher values.

In the lower panel of Figure 9 we compare the eccentricity distribution of planets within the range of semi-major axes:  $0.1 - 1\text{AU}$ ,  $\leq 0.1\text{AU}$  and  $\geq 1\text{AU}$ . Interestingly, we find that the eccentricity distribution of giant planets in the radial range  $0.1 - 1\text{AU}$  is consistent with that of planets at radii larger than  $1\text{AU}$ . A K-S test on these distributions gave a  $p$ -value of 0.31 implying that the two samples are consistent with being taken from the same distribution. For comparison, the same test between the distribution of planets with  $a > 1\text{AU}$  and giant planets at  $a < 0.1\text{AU}$  gave a  $p$ -value of  $\sim 10^{-5}$ . Hence the observed  $e$ -distribution provides no evidence for differences in the eccentricity distribution of WJs and Jupiters outside  $1\text{AU}$  that is expected on the basis of theoretical models. In addition, comparing the eccentricity distribution of all WJs with that of only WJs with one outer companion (orange curve) shows that these two distributions are not significantly different from each other. All these results point either to disk migration (Goldreich & Tremaine 1980) or to in-situ formation (Batygin et al. 2015; Boley et al. 2016) for

the origin of WJs rather than secular migration processes such as the LK mechanism (Dawson & Chiang 2014) or secular chaos (Wu & Lithwick 2011).

## 7. DISCUSSIONS AND CONCLUSIONS

We have considered the population of giant planets in the period valley. These planets, often referred to as WJs, have orbital periods larger than 10days but are inferior to the peak of giant planet frequency observed at  $\approx 1\text{AU}$  (Santerne et al. 2015). It has been argued that such planets might not be able to form in-situ. In a widely discussed model for the formation of these planets, large amplitude eccentricity oscillations induced by an external perturber are followed by efficient tidal dissipation which causes the orbit of the inner planet to shrink during close passages by the host star (e.g., Dong et al. 2014; Dawson & Chiang 2014; Frewen & Hansen 2016).

Before summarizing our results we briefly address the importance of selection effects. In fact, when comparing the predictions of our models to observations we have so far neglected the fact that observations might be biased against for example orbits with high eccentricity and/or large semi-major axis. This might affect the inference of the intrinsic orbital distribution of the observed planets (e.g., Socrates et al. 2012).

We have considered mostly RV data from the exoplanets.org database. RV data might be biased against the detection of longer period planets, although this effect is likely to be small for the semi-major axis range considered here  $a < 1\text{AU}$  (Cumming 2004). More important might be the bias against the detection of eccentric planets which would affect the distributions of Figure 9. In fact, the sparse sampling of an orbit with a high-eccentricity can miss the reflex velocity signal near periastris, leading to non-detection of planets that would be detected at the same semi-major axis and lower eccentricity (Cumming 2004). We believe however that these effects should be relatively small since our sample is restricted to giant planets with relatively large masses ( $M \sin I > 0.5M_{\text{Jupiter}}$ ) and small semi-major axes ( $< 1\text{AU}$ ), which should be relatively easy to detect. We note also that other studies which have taken into account such selection effects have reported results similar to ours, pointing out the excess of highly eccentric WJs predicted by high- $e$  scenarios compared to the observed distribution (Dawson et al. 2015; Frewen & Hansen 2016).

We also note that we have limited the parameter space of our simulations by keeping the perturber mass within  $17M_{\text{Jupiter}}$ . However, the WJs for which there is no observational evidence for a Jupiter companion might be migrating due to interactions with a distant stellar companion. Petrovich (2015) and Anderson et al. (2015) conducted octupole-level population synthesis studies of giant planets migrating through the LK mechanism due to a stellar companion and friction due to tides. Although their initial conditions are different from ours, the fraction of migrating planets obtained in these studies and their orbital distribution are comparable to what is obtained in our study. For example, the fraction ( $\sim 1\%$ ) and orbits of migrating planets displayed in Figure 10 of Petrovich (2015) are clearly similar to those shown in our Figure 5. This suggests that while the perturber plays the fundamental role in inducing the planetary LK oscillations, the perturber properties are likely to not impact

our general results. The main results of our paper should therefore apply also to the case in which the LK oscillations are induced by a stellar companion rather than an outer Jovian companion.

In conclusion we have presented a numerical study of the dynamics of giant planets with close friends. We used both a secular code based on orbit average equations of motion as well as direct three body integrations to address whether the giant planets observed in the semi-major axis range  $0.1 - 1\text{AU}$  could have been formed farther out and then migrated to these radii through secular migration processes such as LK cycles or secular chaos. The main results of our study are summarized below:

- 1 according to the high- $e$  migration hypothesis, HJs and WJs formed originally at  $\gtrsim 1\text{AU}$  distance from their host star. In order to test this hypothesis we addressed whether the observed Jupiter pairs hosting HJs and WJs would be dynamically stable if the inner planet was placed on an eccentric orbit (as required for efficient tidal dissipation) at  $\gtrsim 1\text{AU}$ . According to stability criteria that we have taken from the literature, only four of the twenty-four observed systems would be dynamically stable at these radii with fourteen of them being on intersecting orbits. As we also confirmed by direct integrations, if a planet pairs is unstable, it does not lead to the formation of tidally migrating planets but rather to collisions with the host star or planet ejections. These findings point against a high- $e$  migration scenario from  $\gtrsim 1\text{AU}$  for the formation of most observed systems.
- 2 We showed that high- $e$  migration models for WJs produce a period distribution that is not consistent with observations. By comparing the ratio of WJs to CJs we found in our simulations to that ratio as observed, we infer that  $\lesssim 10\%$  of all gas giants observed at  $0.1 - 1\text{AU}$  from their stellar host could have formed through high- $e$  migration LK processes. Preliminary simulations of systems containing three to five planets suggest that the fraction of WJs produced in multi-planet systems is likely to be small as well.
- 3 Our analysis shows that high- $e$  migration processes tend to produce more HJs than WJs. Accordingly, for any detected WJ with a close companion there should be at least an equal amount of detected HJs also with a close companion. In contrast with this prediction, and restricting ourself to Jupiters discovered through RV surveys, we find that only 2 HJs have a detected outer giant companion within  $\lesssim 5\text{AU}$ , while 20 of the 74 period valley gas gi-

ants do. This points towards a different formation history for the two populations of planets.

- 4 Using both numerical and analytic techniques we have shown that a tidal migration model produces an eccentricity distribution for the migrating planets that also appears to be inconsistent with observations. The oscillations required to produce inward migration tend to excite the eccentricities of migrating planets to values higher than those observed.
- 5 We showed that the observed eccentricity distribution of giant planets in the radial range  $0.1 - 1\text{AU}$  is consistent with the eccentricity distribution for planets at radii larger than  $1\text{AU}$ . This might indicate a close relation between the two populations of planets and perhaps a common formation history.

Based on these results, we conclude that rather than starting on highly-eccentric orbits with orbital periods above 1 year, the Jupiters observed in the radial range  $0.1 - 1\text{AU}$  from their stellar host are likely to have reached the region where they are observed today without tidal circularization. Tidal migration following planet-planet scattering is also disfavored given that we would not expect it to typically result in close and mildly eccentric companions to WJs (Nagasawa et al. 2008; Beaugé & Nesvorný 2012).

Where do the WJs come from then? Our results may indicate that disk migration is the dominant channel for producing WJs. Alternatively, they might have formed in-situ (Huang et al. 2016), i.e., they underwent runaway gas accretion, from originally low-mass closely packed planets (e.g., Lee et al. 2014). However, both disk migration and in-situ formation are more likely to produce planets on nearly circular and low inclined orbits, so it remains to be explained how in these scenarios the planets eccentricities could have been excited to the observed values. A possibility is that the eccentricities were excited through secular chaos (Wu & Lithwick 2011), which could imply the presence of one or multiple still undetected planet companions to the numerous planet pairs observed in the period valley.<sup>1</sup>

We thank Bekki Dawson and Eugene Chiang for useful suggestions, and the referee for their detailed comments that helped to improve the paper. FA acknowledges support from a CIERA postdoctoral fellowship at Northwestern University. ASH was supported by the Netherlands Research Council NWO (grants 639.073.803 [VICI], 614.061.608 [AMUSE] and 612.071.305 [LGM]) and the Netherlands Research School for Astronomy (NOVA). YL acknowledges grant AST-1352369 from NSF and NNX14AD21G from NASA.

## REFERENCES

- Anderson, K. R., Storch, N. I., & Lai, D. 2015, arXiv:1510.08918  
 Antonini, F., Murray, N., & Mikkola, S. 2014, *ApJ*, 781, 45
- <sup>1</sup> As this paper was submitted, we became aware of a similar study by Petrovich & Tremaine (2016). Based on a population-synthesis study similar to ours Petrovich & Tremaine (2016) conclude that high-eccentricity migration excited by an outer planetary companion can account at most for  $\sim 20\%$  of the warm Jupiters, a fraction twice as large as the upper limit found here.
- Antonini, F., & Perets, H. B. 2012, *ApJ*, 757, 27  
 Batygin, K., Bodenheimer, P. H., & Laughlin, G. P. 2015, arXiv:1511.09157  
 Beaugé, C., & Nesvorný, D. 2012, *ApJ*, 751, 119  
 Blaes, O., Lee, M. H., & Socrates, A. 2002, *ApJ*, 578, 775  
 Boley, A. C., Granados Contreras, A. P., & Gladman, B. 2016, *ApJ*, 817, L17  
 Correia, A. C. M., Udry, S., Mayor, M., et al. 2005, *A&A*, 440, 751

- Cumming, A. 2004, MNRAS, 354, 1165
- Dawson, R. I., & Murray-Clay, R. A. 2013, ApJ, 767, L24
- Dawson, R. I., & Chiang, E. 2014, Science, 346, 212
- Dawson, R. I., Murray-Clay, R. A., & Johnson, J. A. 2015, ApJ, 798, 66
- Desort, M., Lagrange, A.-M., Galland, F., et al. 2008, A&A, 491, 883
- Dong, S., Katz, B., & Socrates, A. 2014, ApJ, 781, L5
- Eggleton, P., & Kiseleva, L. 1995, ApJ, 455, 640
- Endl, M., Caldwell, D. A., Barclay, T., et al. 2014, ApJ, 795, 151
- Frewen, S. F. N., & Hansen, B. M. S. 2016, MNRAS, 455, 1538
- Giguere, M. J., Fischer, D. A., Howard, A. W., et al. 2012, ApJ, 744, 4
- Goldreich, P., & Tremaine, S. 1980, ApJ, 241, 425
- Haghighipour, N., Butler, R. P., Rivera, E. J., Henry, G. W., & Vogt, S. S. 2012, ApJ, 756, 91
- Hamers, A. S., Perets, H. B., Antonini, F., & Portegies Zwart, S. F. 2015, MNRAS, 449, 4221
- Hamers, A. S., & Portegies Zwart, S. F. 2015, arXiv:1511.00944
- Hébrard, G., Bonfils, X., Ségransan, D., et al. 2010, A&A, 513, A69
- Huang, C. X., Wu, Y., & Triaud, A. H. M. J. 2016, arXiv:1601.05095
- Hut, P. 1981, A&A, 99, 126
- Jones, H. R. A., Butler, R. P., Tinney, C. G., et al. 2010, MNRAS, 403, 1703
- Lee, E. J., Chiang, E., & Ormel, C. W. 2014, ApJ, 797, 95
- Lin, D. N. C., Bodenheimer, P., & Richardson, D. C. 1996, Nature, 380, 606
- Mardling, R. A., & Aarseth, S. J. 2001, MNRAS, 321, 398
- Matsumura, S., Thommes, E. W., Chatterjee, S., & Rasio, F. A. 2010, ApJ, 714, 194
- Mayor, M., Udry, S., Naef, D., et al. 2004, A&A, 415, 391
- Merritt, D., Dynamics and Evolution of Galactic Nuclei, 2013, Princeton University Press
- Meschiari, S., Laughlin, G., Vogt, S. S., et al. 2011, ApJ, 727, 117
- Mikkola, S., & Merritt, D. 2006, MNRAS, 372, 219
- Mikkola, S., & Merritt, D. 2008, AJ, 135, 2398
- Moorhead, A. V., Ford, E. B., Morehead, R. C., et al. 2011, ApJS, 197, 1
- Moutou, C., Hébrard, G., Bouchy, F., et al. 2014, A&A, 563, A22
- Nagasawa, M., Ida, S., & Bessho, T. 2008, ApJ, 678, 498-508
- Naoz, S., Farr, W. M., Lithwick, Y., Rasio, F. A., & Teyssandier, J. 2011, Nature, 473, 187
- Niedzielski, A., Villaver, E., Wolszczan, A., et al. 2015, A&A, 573, A36
- Petrovich, C. 2015, ApJ, 808, 120
- Petrovich, C. 2015, ApJ, 799, 27
- Petrovich, C., & Tremaine, S. 2016, arXiv:1604.00010
- Pilyavsky, G., Mahadevan, S., Kane, S. R., et al. 2011, ApJ, 743, 162
- Quinn, S. N., White, T. R., Latham, D. W., et al. 2015, ApJ, 803, 49
- Rasio, F. A., & Ford, E. B. 1996, Science, 274, 954
- Robertson, P., Endl, M., Cochran, W. D., et al. 2012, ApJ, 749, 39
- Santerne, A., Moutou, C., Tsantaki, M., et al. 2015, arXiv:1511.00643
- Ségransan, D., Udry, S., Mayor, M., et al. 2010, A&A, 511, A45
- Socrates, A., Katz, B., & Dong, S. 2012, arXiv:1209.5724
- Socrates, A., Katz, B., Dong, S., & Tremaine, S. 2012, ApJ, 750, 106
- Tan, X., Payne, M. J., Lee, M. H., et al. 2013, ApJ, 777, 101
- Tinney, C. G., Butler, R. P., Marcy, G. W., et al. 2006, ApJ, 647, 594
- Wang, X., Sharon, Wright, J. T., Cochran, W., et al. 2012, ApJ, 761, 46
- Winn, J. N., Johnson, J. A., Howard, A. W., et al. 2010, ApJ, 718, 575
- Wright, J. T., Upadhyay, S., Marcy, G. W., et al. 2009, ApJ, 693, 1084
- Wright, J. T., Fakhouri, O., Marcy, G. W., et al. 2011, PASP, 123, 412
- Wright, J. T., Marcy, G. W., Howard, A. W., et al. 2012, ApJ, 753, 160
- Wu, Y., & Murray, N. 2003, ApJ, 589, 605
- Wu, Y., & Lithwick, Y. 2011, ApJ, 735, 109